


 Cite this: *CrystEngComm*, 2018, 20, 402

 Received 24th November 2017,  
Accepted 3rd January 2018

DOI: 10.1039/c7ce02034a

[rsc.li/crystengcomm](http://rsc.li/crystengcomm)

## Insight into the reversible structural crystalline-state transformation from MIL-53(Al) to MIL-68(Al)<sup>†</sup>

 Adelaida Perea-Cachero, <sup>a</sup> Enrique Romero,<sup>b</sup>  
Carlos Téllez <sup>\*a</sup> and Joaquín Coronas <sup>a</sup>

The reversible crystalline transformation between MIL-53(Al) and MIL-68(Al) is described. This followed a uniform conversion model with cleavage and formation of metal–ligand bonds after exchange or removal of guest molecules. MIL-68(Al) materials produced during the transformations had higher thermal stability and crystallinity than the as-synthesized MIL-68(Al).

Metal–organic frameworks (MOFs) have gained much attention in the last decade owing to their exceptional properties leading to a widespread range of applications, *e.g.* gas adsorption, gas separation and storage, catalysis, thin film devices, luminescence, magnetism and conductivity.<sup>1–6</sup> Their remarkable properties comprise large pore volumes and surface areas, permanent porosity, chemical and structural diversity, a wide range of pore sizes, high thermal and chemical stabilities, and structural flexibility.<sup>3,7–12</sup> The molecular design of MOFs is a tool to tune the framework structures and achieve different network topologies which influences their properties and applications.<sup>11</sup> The structural flexibility of MOFs is reflected in changes in the coordination number and geometry, dimensionality, chirality, interpenetration, topology, *etc.*, through the breaking and forming of coordination and/or covalent bonds<sup>13,14</sup> after different external stimuli (temperature, pressure, removal or exchange of guest molecules, light, heat, post-synthetic modification, mechanochemical force, *etc.*).<sup>13,15–18</sup>

In this regard, single-crystal to single-crystal transformations (SC–SC) of MOFs have attracted recent interest because the physical–chemical changes in the framework can be accu-

rately associated to the structural and property changes before and after the stimulus action.<sup>14,18,19</sup> However, obtaining a perfect single-crystal is not a trivial issue, as crystal growth and post-synthetic processes damage crystals.<sup>14</sup> In addition, crystals can barely maintain their single crystallinity when suffering a drastic solid-state rearrangement of atoms.<sup>17,18</sup> Single-crystal X-ray diffraction (SCXRD) provides valuable information about crystalline-state transformations.<sup>14</sup> When single-crystals are not available, alternative techniques (powder X-ray diffraction (PXRD), thermogravimetric analysis, infrared spectroscopy, Raman spectroscopy, atomic force microscopy, *etc.*) are needed to properly describe the crystalline-state transformations.<sup>13,20</sup>

MOFs MIL-68 (Kagomé topology)<sup>21</sup> and MIL-53 (sra topology with 4<sup>4</sup>-nets)<sup>22,23</sup> are polymorphs when their pores are empty.<sup>24</sup> MIL-68 and MIL-53 structures are constructed from infinite chains of inorganic MO<sub>4</sub>(OH)<sub>2</sub> (M, metal) octahedra linked by the apical *trans* hydroxyl functions.<sup>25,26</sup> Two consecutive octahedra are linked by two carboxylate groups.<sup>26</sup> Octahedral chains are connected by terephthalate ligands to create one-dimensional channels.<sup>25,26</sup> MIL-68 presents triangular as well as hexagonal channels (6.0–6.4 and 16–17 Å, respectively),<sup>21,26,27</sup> while MIL-53 only has rhombic cavities (*ca.* 8.5 Å).<sup>19,25</sup> MIL-68 and MIL-53 represent good examples of rigid and flexible MOF frameworks, respectively. The process related to the structural flexibility of MIL-53, commonly called breathing, is considered as a crystalline-state transformation where the structure reversibly shrinks or expands in the presence of guests.<sup>13,19</sup> When MIL-53(Al) is synthesized, known as MIL-53(Al)<sub>as</sub> (as-synthesized), its structure contains disordered terephthalic acid (TPA) molecules in the pores.<sup>19</sup> The calcination of MIL-53(Al)<sub>as</sub> leads to the removal of the TPA, achieving the MIL-53(Al)<sub>lp</sub> (large-pore) form with empty and enlarged pores.<sup>19</sup> On exposure of MIL-53(Al)<sub>lp</sub> to air, the framework adsorbs water molecules, leading to pore contraction and giving the MIL-53(Al)<sub>np</sub> (narrow-pore) phase.<sup>19</sup>

Some interesting structural transformations related to MIL-type materials have recently been reported. The

<sup>a</sup> Chemical and Environmental Engineering Department, Instituto de Nanociencia de Aragón (INA), Universidad de Zaragoza, 50018 Zaragoza, Spain.  
E-mail: ctellez@unizar.es

<sup>b</sup> Chemical and Environmental Engineering Department, Instituto de Investigación en Ingeniería de Aragón (I3A), Universidad de Zaragoza, 50018 Zaragoza, Spain

<sup>†</sup> Electronic supplementary information (ESI) available: Experimental section, FTIR spectra, TGA and DTG curves, N<sub>2</sub> sorption isotherms and additional PXRD patterns and SEM images. See DOI: 10.1039/c7ce02034a

topological isomers MIL-101(V) and MIL-88B(V) converted into MIL-47 upon heating at 200 °C in ethanol or in an ethanol/HCl solution.<sup>28</sup> The structural and morphological transformation of MIL-68(In) to QMOF-2 by a thermal treatment (100 °C) in the presence of an excess of TPA (dissolved in *N,N*-dimethylformamide, DMF).<sup>29</sup> The crystal growth of NH<sub>2</sub>-MOF-235 in a solution of Al<sup>3+</sup> and terephthalate ions in DMF led to the formation of NH<sub>2</sub>-MIL-101(Al) when the temperature was increased.<sup>30</sup> NH<sub>2</sub>-MIL-88B(Fe) can undergo a reversible transformation into NH<sub>2</sub>-MIL-53(Fe) upon caffeine encapsulation and release.<sup>31</sup>

In this work, the reversible transformation from MIL-53(Al) into MIL-68(Al) was accomplished following two paths (see Fig. 1): (1) from MIL-53(Al)as and (2) from MIL-53(Al)np. MIL-53(Al) materials were soaked in DMF at 130 °C under reflux and stirring for 3 d, leading to MIL-68(Al)<sub>1</sub> and MIL-68(Al)<sub>2</sub>, respectively. Then, both MIL-68(Al)s were outgassed at 260 °C for 1 d and, after exposure to the environment, the np phase of MIL-53(Al) was achieved (MIL-53(Al)np<sub>1</sub> and MIL-53(Al)np<sub>2</sub>, respectively).

As observed by scanning electron microscopy (SEM, Fig. 2), MIL-53(Al)as crystals (5–10 μm in size) do not have the typical shape of elongated hexagonal prisms (Fig. 2a).<sup>33</sup> When MIL-53(Al)as was calcined at 330 °C for 3 d, the resulting MIL-53(Al)np maintained the initial shape, although some crystals were broken leading to small particles on their surface (Fig. 2d). When transforming MIL-53(Al) into MIL-68(Al) and MIL-68(Al) into MIL-53(Al)np, the shape and size of the crystals were preserved (first and second rows from bottom in Fig. 2). Nonetheless, several crystals were broken, probably due to the stirring action during the immersion in DMF.

Because the crystal size was not appropriate for performing SCXRD, PXRD was used to characterize the crystalline structure of the samples (Fig. 3). The MIL-68(Al)<sub>1</sub> and MIL-68(Al)<sub>2</sub> curves agree well with that of MIL-68(Al)as powder. The presence of the peak at  $2\theta = 4.8^\circ$  in MIL-68(Al)as, but not in MIL-68(Al)<sub>1</sub> and MIL-68(Al)<sub>2</sub>, is related to certain

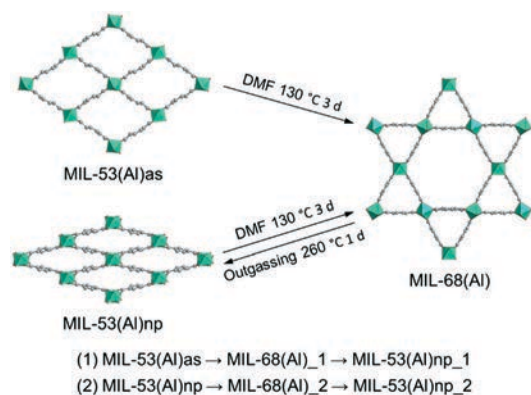


Fig. 1 Schematic representation of the reversible transformation from MIL-53(Al) to MIL-68(Al). Molecular graphics were done with Diamond<sup>32</sup> using the cif files of MIL-68(Sc),<sup>6</sup> MIL-53(Al)as (CCDC 220475)<sup>19</sup> and MIL-53(Al)np (CCDC 220477).<sup>19</sup>

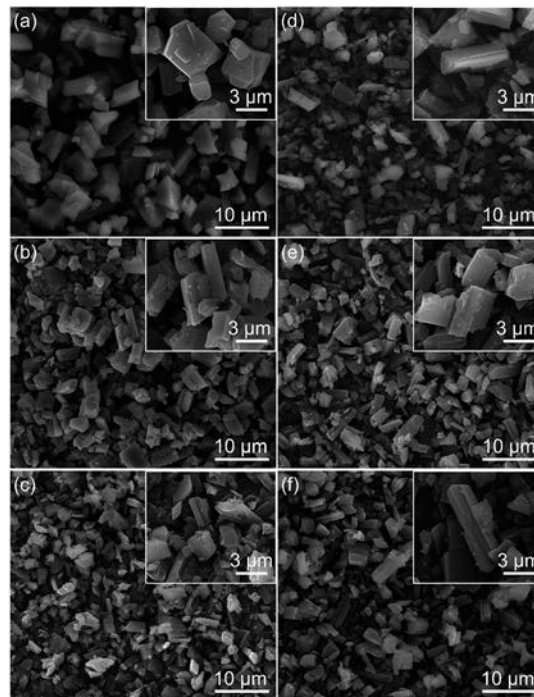


Fig. 2 SEM images of (a) MIL-53(Al)as, (b) MIL-68(Al)<sub>1</sub>, (c) MIL-53(Al)np<sub>1</sub>, (d) MIL-53(Al)np, (e) MIL-68(Al)<sub>2</sub> and (f) MIL-53(Al)np<sub>2</sub>.

preferential orientation of crystals which changes are due to the different particle size and shape of the MIL-68(Al)s. As seen by SEM, needles of MIL-68(Al)as (*ca.* 1.25 μm in size) are randomly oriented forming spherical aggregates (Fig. S1a†), whereas prisms of MIL-68(Al)<sub>1</sub> and MIL-68(Al)<sub>2</sub> have this certain preferential orientation due to their larger faces (*b* axis parallel to the sample holder, Fig. 2),<sup>33</sup> leading to the disappearance of the above-mentioned reflection (the plane corresponding to the peak is not seen in the MIL-68(Al) crystals with the shape and size of MIL-53(Al)). This lack of peaks in the XRD has been previously observed in oriented crystals

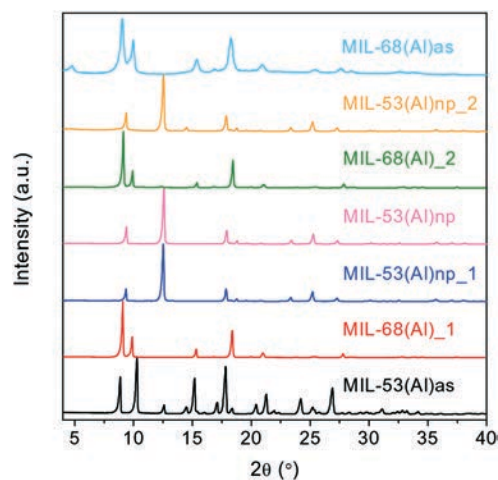


Fig. 3 PXRD patterns of the products of the reversible transformation from MIL-53(Al) to MIL-68(Al) and that of MIL-68(Al)as.

of MOFs grown on supports.<sup>34</sup> In agreement with this, MIL-68(Al)<sub>1</sub> and MIL-68(Al)<sub>2</sub> are more crystalline than MIL-68(Al)<sub>as</sub> and the peaks are narrower since the crystals are larger. Besides, MIL-53(Al)np<sub>1</sub> and MIL-53(Al)np<sub>2</sub> feature the MIL-53(Al)np structure. The PXRD characterization confirms that both transformations were totally reversible and that crystallinity was preserved. The observed amorphization by Panda *et al.*<sup>35</sup> in another kind of MOFs has not been detected during our transformation which does not rule out that this happens as a rapid transition to a crystalline phase.

Since MIL-53 and MIL-68 are polymorphs, similar Fourier transform infrared (FTIR) spectra were expected although they could be readily differentiated and identified by means of this technique (see Fig. S2†). The spectra of MIL-68(Al)<sub>1</sub> and MIL-68(Al)<sub>2</sub> are consistent with the spectrum of MIL-68(Al)<sub>as</sub> and indicate the presence of DMF and some TPA molecules in the pores (bands of the carbonyl groups (C=O) at 1674 and 1701 cm<sup>-1</sup>, respectively). The presence of TPA in MIL-68(Al)<sub>1</sub> is ascribed to a non-complete elimination from the pores of MIL-53(Al)<sub>as</sub> by solution with DMF. In MIL-68(Al)<sub>2</sub>, it is assigned to a small residual amount of TPA coming from MIL-53(Al)np. The spectra of MIL-53(Al)np<sub>1</sub> and MIL-53(Al)np<sub>2</sub> match that of MIL-53(Al)np. The weak band at 1699 cm<sup>-1</sup> in MIL-53(Al)np<sub>2</sub> points to a partial removal of TPA when MIL-68(Al)<sub>2</sub> was outgassed.

Fig. S3† shows the thermogravimetric analysis (TGA) and differential thermogravimetric (DTG) curves in air of the products obtained in this work. The weight-losses are detailed in the Fig. S3† caption. Upon treatment in DMF, MIL-53(Al)<sub>as</sub> and MIL-53(Al)np transform into MIL-68(Al) (MIL-68(Al)<sub>1</sub> and MIL-68(Al)<sub>2</sub>) containing around 1% of TPA. The outgassing at high temperature gives rise unequivocally to MIL-53(Al)np networks (MIL-53(Al)np<sub>1</sub> and MIL-53(Al)np<sub>2</sub>). In the case of MIL-53(Al)np<sub>2</sub>, the outgassing process (260 °C for 1 d) does not completely eliminate the TPA trapped in MIL-68(Al)<sub>2</sub> (a small step of 0.5% at 300–370 °C is seen in the thermogram of MIL-53(Al)np<sub>2</sub>). It is worth mentioning that the framework stability of the MIL-68(Al) products (MIL-68(Al)<sub>1</sub> and MIL-68(Al)<sub>2</sub>) is as high as that of MIL-53(Al), achieving a thermal improvement of 50 °C (from 430 °C in MIL-68(Al)<sub>as</sub> to 480 °C in MIL-53(Al) (as and np)), in such a way that the stability was not affected by the distinct processes performed to achieve the final MIL-53(Al)np compounds (outgassing and immersion in DMF at high temperature). This could be related to the crystal size. Larger crystals have a higher mass transport resistance, hindering their decomposition process<sup>36</sup> and, in the case of porous materials, delaying the removal of trapped molecules.<sup>37</sup>

Nuclear magnetic resonance (NMR) spectra of the MIL-53(Al)np and MIL-53(Al)np<sub>2</sub> samples were taken to study the reversibility of the transformation in depth. The <sup>13</sup>C cross polarization-magic angle spinning (CP-MAS) NMR spectra are depicted in Fig. S4†. The strong and weak signals in MIL-68(Al)<sub>as</sub> and MIL-53(Al)np<sub>2</sub>, respectively, at 170 ppm are due to the carbon of the carboxylic (-COOH) groups from both guests and ligands.<sup>19</sup> As confirmed by FTIR (Fig. S2†) and

TGA (Fig. S3†), MIL-68(Al)<sub>as</sub> barely contained TPA molecules in its pores, indicating that this signal is mainly produced by the carboxylates. The weak signal in MIL-53(Al)np<sub>2</sub> at 170 ppm is ascribed to the carboxylic groups of the small amount of free TPA, in agreement with the TGA discussed above.

The products of the transformations (MIL-68(Al)<sub>2</sub>, MIL-53(Al)np<sub>2</sub> and MIL-53(Al)np<sub>1</sub>) present type I isotherms, like MIL-68(Al)<sub>as</sub> and MIL-53(Al)np, so that they retained their microporosity (Fig. S5†). MIL-53(Al)np<sub>1</sub> and MIL-53(Al)np<sub>2</sub> (1253 and 1167 m<sup>2</sup> g<sup>-1</sup>, respectively) exceed the BET specific surface areas of MIL-68(Al)<sub>as</sub> and MIL-53(Al)np (1121 and 1051 m<sup>2</sup> g<sup>-1</sup>, respectively). In most cases, the BET specific surface areas of both MIL-53(Al)np<sub>1</sub> and MIL-53(Al)np<sub>2</sub> are also higher than those of the MIL-53(Al)np materials reported in the literature (819–1235 m<sup>2</sup> g<sup>-1</sup>, Table S1†). The outgassing at 260 °C for 1 d was effective enough to achieve a higher degree of activation. Despite this, MIL-53(Al)np<sub>2</sub> contained still a small amount of TPA, as observed by FTIR, TGA and NMR, leading to a lower BET surface area than that of MIL-53(Al)np<sub>1</sub>. MIL-68(Al)<sub>2</sub> had the lowest BET surface area (391 m<sup>2</sup> g<sup>-1</sup>) due to the unsuccessful removal of DMF molecules during the outgassing prior to the sorption measurements.

It is worth mentioning that when MIL-68(Al)<sub>as</sub> was used to achieve the transformation from MIL-68(Al) to MIL-53(Al) under the same conditions (outgassing, 260 °C), the product after the conversion was MIL-53(Al)lp instead of MIL-53(Al)np (Fig. S6†). This may be due to the lower crystallinity of MIL-68(Al)<sub>as</sub> and, thus, the outgassed products. The lower order in lattice would impede the contraction of the structure upon water adsorption from the environment. The reaction was not completed after 24 h and the products after outgassing for 8, 16 and 24 h lost crystallinity (Fig. S1b and S6†), probably due to the smaller crystal size of MIL-68(Al)<sub>as</sub> (*ca.* 1.25 μm) in comparison with that of MIL-68(Al)<sub>1</sub> and MIL-68(Al)<sub>2</sub> (*ca.* 5–10 μm).

Fig. 4 displays the suggested mechanism for the transformations between MIL-53(Al) and MIL-68(Al). It is thought that when DMF entered the pores of MIL-53(Al)<sub>as</sub> and MIL-53(Al)np, it replaced and dissolved water and TPA, respectively. DMF molecules have been reported to serve as templates for the formation of the triangular pores of MIL-68,<sup>24</sup> so that DMF molecules strongly react with the acute vertex of the rhombic MIL-53(Al) pores. Some Al-terephthalate bonds broke and new ones were created, forming triangular channels by dividing the rhombic channels through the obtuse vertices and enclosing DMF molecules (Fig. 4a). The steric hindrance provoked a general structural movement of expansion in two steps. First, the inorganic octahedral chains were aligned to originate hexagonal cavities in such a way that rows of hexagonal and triangular pores were alternated (Fig. 4b). Second, every other hexagon centre in the same row was occupied by the adjacent inorganic chain linking two triangular channels (Fig. 4c). This involved the breakage and formation of metal-ligand bonds. The result was a rearrangement of the inorganic chains and ligands to give

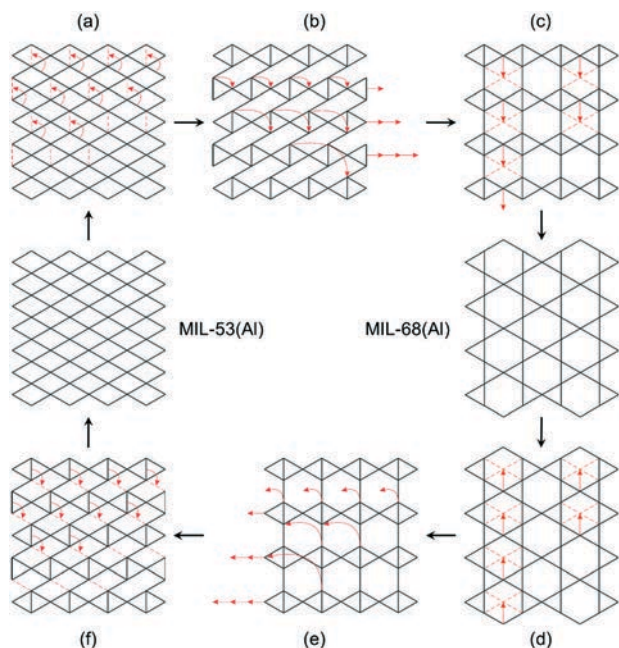


Fig. 4 Schematic mechanism proposed for the reversible transformation from MIL-53(Al) to MIL-68(Al). a–f indicate different states of the transformation.

the Kagomé topology of MIL-68(Al) with the triangular pores filled with DMF molecules. The transformation from MIL-68(Al) to MIL-53(Al)<sub>np</sub> followed the inverse mechanism. Since outgassing removed the DMF molecules, the triangular pores became empty and unstable. Inorganic chains linking two triangular channels from alternate columns moved to adjacent hexagon centres with the consequent breakage of the coordination bonds (Fig. 4d). New metal–ligand bonds were formed with the free one-end ligands. The inorganic chains moved to occupy the hexagon centres in such a way that a structural contraction was induced (Fig. 4e). Finally, terephthalate anions splitting the rhombi broke one of the coordination bonds and closed the open rhombic channels through a new linkage to other octahedral chains to yield the *sra* topology of MIL-53(Al) (Fig. 4f). It is thought that the MIL-53(Al)<sub>lp</sub> phase was initially achieved, but the water adsorption from the environment shrunk the pores and led to the MIL-53(Al)<sub>np</sub> form. According to the SEM images, the reversible transformation followed a uniform conversion model where the rearrangement reactions were produced simultaneously over the whole crystal to generate MIL-68(Al) or MIL-53(Al). It is worth remembering that the MIL-type crystals preserved their size, shape and crystallinity in spite of the breakage and formation of coordination bonds caused by the exchange and removal of guests.

In summary, the reversible crystalline-state transformation between the *sra* and Kagomé topologies of the polymorphs MIL-53(Al) and MIL-68(Al), respectively, is reported. The transformation was caused by the exchange or removal of guest molecules from the pores, giving rise to reorganization reactions through the cleavage and formation of coordination bonds. The transformation followed a uniform conversion

model where crystals were not damaged. The process gave highly crystalline MIL-68(Al) with improved thermal stability. The structural interconversion capability between MIL-53(Al) and MIL-68(Al) following an external stimulus enables their use as smart materials in molecular recognition, guest exchange and sensors.

Financial support from the Spanish Ministry of Economy and Competitiveness (MINECO) and European Regional Development Fund (MAT2013-40556-R, MAT2016-77290-R), ESF and the Aragón Government (DGA, T05) is gratefully acknowledged. A. P.-C. also thanks the DGA for a Ph.D. grant. The authors would like to acknowledge the use of the Servicio General de Apoyo a la Investigación-SAI (Universidad de Zaragoza (UZ)) and the Laboratorio de Microscopías Avanzadas at INA (LMA-INA, UZ).

## Conflicts of interest

There are no conflicts to declare.

## Notes and references

- D. Y. Hong, Y. K. Hwang, C. Serre, G. Férey and J. S. Chang, *Adv. Funct. Mater.*, 2009, **19**, 1537–1552.
- H.-C. Zhou, J. R. Long and O. M. Yaghi, *Chem. Rev.*, 2012, **112**, 673–674.
- J. E. Mondloch, O. Karagiari, O. K. Farha and J. T. Hupp, *CrystEngComm*, 2013, **15**, 9258–9264.
- A. Perea-Cachero, P. Calvo, E. Romero, C. Tellez and J. Coronas, *Eur. J. Inorg. Chem.*, 2017, 2532–2540.
- J. Cookney, W. Ogieglo, P. Hrabanek, I. Vankelecom, V. Fila and N. Benes, *Chem. Commun.*, 2014, **50**, 11698–11700.
- L. Mitchell, B. Gonzalez-Santiago, J. P. S. Mowat, M. E. Gunn, P. Williamson, N. Acerbi, M. L. Clarke and P. A. Wright, *Catal. Sci. Technol.*, 2013, **3**, 606–617.
- J. Cravillon, R. Nayuk, S. Springer, A. Feldhoff, K. Huber and M. Wiebcke, *Chem. Mater.*, 2011, **23**, 2130–2141.
- M. Shah, M. C. McCarthy, S. Sachdeva, A. K. Lee and H.-K. Jeong, *Ind. Eng. Chem. Res.*, 2012, **51**, 2179–2199.
- G. Yilmaz, A. Ozcan and S. Keskin, *Mol. Simul.*, 2015, **41**, 713–726.
- B. Seoane, S. Sorribas, A. Mayoral, C. Tellez and J. Coronas, *Microporous Mesoporous Mater.*, 2015, **203**, 17–23.
- Y. X. Sun, Y. Y. Sun, H. Zheng, H. L. Wang, Y. Han, Y. Yang and L. Wang, *CrystEngComm*, 2016, **18**, 8664–8671.
- K. Liu, X. Li, D. X. Ma, Y. Han, B. Y. Li, Z. Shi, Z. J. Li and L. Wang, *Mater. Chem. Front.*, 2017, **1**, 1982–1988.
- G. K. Kole and J. J. Vittal, *Chem. Soc. Rev.*, 2013, **42**, 1755–1775.
- J. P. Zhang, P. Q. Liao, H. L. Zhou, R. B. Lin and X. M. Chen, *Chem. Soc. Rev.*, 2014, **43**, 5789–5814.
- L. J. Barbour, *Aust. J. Chem.*, 2006, **59**, 595–596.
- S. R. Zheng, S. L. Cai, M. Pan, J. Fan, T. Xiao and W. G. Zhang, *CrystEngComm*, 2011, **13**, 883–888.
- A. Calderon-Casado, G. Barandika, B. Bazan, M.-K. Urriaga, O. Vallcorba, J. Rius, C. Miravittles and M.-I. Arriortua, *CrystEngComm*, 2011, **13**, 6831–6838.

- 18 D. X. Xue, W. X. Zhang, X. M. Chen and H. Z. Wang, *Chem. Commun.*, 2008, 1551–1553.
- 19 T. Loiseau, C. Serre, C. Huguenard, G. Fink, F. Taulelle, M. Henry, T. Bataille and G. Ferey, *Chem. – Eur. J.*, 2004, **10**, 1373–1382.
- 20 T. L. Threlfall, *Analyst*, 1995, **120**, 2435–2460.
- 21 C. Volklinger, M. Meddouri, T. Loiseau, N. Guillou, J. Marrot, G. Ferey, M. Haouas, F. Taulelle, N. Audebrand and M. Latroche, *Inorg. Chem.*, 2008, **47**, 11892–11901.
- 22 N. L. Rosi, J. Kim, M. Eddaoudi, B. L. Chen, M. O’Keeffe and O. M. Yaghi, *J. Am. Chem. Soc.*, 2005, **127**, 1504–1518.
- 23 Y. Zhu, M. Zhu, L. Xia, Y. L. Wu, H. Hua and J. M. Xie, *Sci. Rep.*, 2016, **6**, 29728.
- 24 A. Fateeva, P. Horcajada, T. Devic, C. Serre, J. Marrot, J.-M. Greneche, M. Morcrette, J. M. Tarascon, G. Maurin and G. Ferey, *Eur. J. Inorg. Chem.*, 2010, 3789–3794.
- 25 C. Serre, F. Millange, C. Thouvenot, M. Nogues, G. Marsolier, D. Louer and G. Ferey, *J. Am. Chem. Soc.*, 2002, **124**, 13519–13526.
- 26 K. Barthelet, J. Marrot, G. Ferey and D. Riou, *Chem. Commun.*, 2004, 520–521.
- 27 Y. Hu, B. Lin, P. He, Y. Y. Li, Y. N. Huang and Y. Song, *Chem. – Eur. J.*, 2015, **21**, 18739–18748.
- 28 F. Carson, J. Su, A. E. Platero-Prats, W. Wan, Y. Yun, L. Samain and X. Zou, *Cryst. Growth Des.*, 2013, **13**, 5036–5044.
- 29 S. Choi, H. J. Lee, T. Kim and M. Oh, *Eur. J. Inorg. Chem.*, 2014, 6220–6224.
- 30 E. Stavitski, M. Goesten, J. Juan-Alcaniz, A. Martinez-Joaristi, P. Serra-Crespo, A. V. Petukhov, J. Gascon and F. Kapteijn, *Angew. Chem., Int. Ed.*, 2011, **50**, 9624–9628.
- 31 N. Liedana, P. Lozano, A. Galve, C. Tellez and J. Coronas, *J. Mater. Chem. B*, 2014, **2**, 1144–1151.
- 32 H. Putz and K. Brandenburg, *Diamond – Crystal and Molecular Structure Visualization*, Brandenburg GbR, Bonn, 2016.
- 33 F. Zhang, X. Zou, F. Sun, H. Ren, Y. Jiang and G. Zhu, *CrystEngComm*, 2012, **14**, 5487–5492.
- 34 C. Scherb, A. Schodel and T. Bein, *Angew. Chem., Int. Ed.*, 2008, **47**, 5777–5779.
- 35 T. Panda, S. Horike, K. Hagi, N. Ogiwara, K. Kadota, T. Itakura, M. Tsujimoto and S. Kitagawa, *Angew. Chem., Int. Ed.*, 2017, **56**, 2413–2417.
- 36 S. Y. Lu, H. Y. Huang and K. H. Wu, *J. Mater. Res.*, 2001, **16**, 3053–3059.
- 37 M. Navarro, E. Mateo, B. Diosdado and J. Coronas, *CrystEngComm*, 2012, **14**, 6016–6022.